

Spatial organization and evolutionary period of the epidemic model using cellular automata

Quan-Xing Liu,^{*} Zhen Jin,[†] and Mao-Xing Liu
*Department of mathematics, North University of China,
 Taiyuan, Shan'xi, 030051, People's Republic of China*
 (Dated: July 22, 2018)

We investigate epidemic models with spatial structure based on the cellular automata method. The construction of the cellular automata is from the study by Weimar and Boon about the reaction-diffusion equations [Phys. Rev. E 49, 1749 (1994)]. Our results show that the spatial epidemic models exhibits spontaneous formation of irregular spiral waves at large scales within the domain of chaos. Moreover the irregular spiral waves grow stably. The system also shows spatial period-2 structure at one dimension outside the domain of chaos. It is interesting that the spatial period-2 structure will break and transform to spatial synchronous configuration in the domain of chaos. Our results confirm that populations embed and disperse more stably in space than they do in non-spatial counterparts.

PACS numbers: 05.50.+q, 87.23.Cc, 87.18.Hf, 89.75.Fb

I. INTRODUCTION

Several theoretical models have shown that population invasion and dispersion is more stable in space than that in non-spatial counterparts. More stable mean that a previously unstable equilibrium point becomes stable under a greater variety of conditions, or that an equilibrium is approached faster [1]. In oscillatory systems where the equilibrium is a limit cycle or more generally an unstable focus, diffusion or dispersal will create wave-like patterns. The Lattice Lotka-Volterra (LLV) model was studied extensively [2, 3, 4]. In non-linear ecology system, the two most commonly seen patterns are spiral waves and turbulence. Spiral waves play an important role in ecological systems. For example, spatially induced speciation prevents extinction for the predator-prey models [5, 6]. A classical epidemic model is ordinary differential equations (ODEs), or called mean-field (MF) approximation [7]. The ODEs methods (or MF) are based on the assumption that the population is well-mixed, with the subpopulations involving susceptible, infected, removed, etc., interacting in proportion to their sizes. Nonspatial theory typically predicts selection for maximal number of secondary infectors. Among these epidemic features, the existence of threshold values is crucial for the spread of an infection [8, 9]. A second classical approach describes spatially extended subpopulations, such as a coupled map-lattice models [10], reaction-diffusion equations, deterministic cellular automata and integrodifference equations model. In the literature [11] the author argues the numerical simulations in a predator-prey system, and shows that there are either irregular spatiotemporal oscillations behind the invasion or regular spatiotemporal oscillations with the form of a periodic travelling ‘wake’ depending

on parameter values.

In our paper, the geographic spread of an epidemic can be analyzed as a reaction-diffusion system, in which both subpopulation exhibit local random movement, and the algorithm of cellular automata are based on these paper [11, 12]. More recently, studies have shown large-scale spatiotemporal patterns in measles [13] and dengue fever [14]. These studies have shed new light onto key research issues in spatial epidemic dynamics, but the detailed theoretical studies are difficult. The study of population dynamics takes into account the species distribution in space, interactions between individual species that are located in the same neighborhood, and mobility of the various species [15, 16, 17]. These studies predict the formation of spatial complex structure, phase transitions, multistability, oscillatory regions, etc. In the Ref. [17], the author studies the susceptible-infected-resistant-susceptible (SIRS) models with spatial structure using cellular automata rules, showing the formation process of the spatial patterns (turbulent waves and stable spiral waves) in the two-dimensional space and existence of stable spiral waves in the SIRS model.

The principal objectives of the present work is that the susceptible-exposed-infected-resistant (SEIR) model with spatial structure is investigated by using cellular automata algorithm. The SEIR model and its classical ODEs version are presented in [18, 19]. In fact, many diseases are seasonal, and therefore an important question for further studies is how seasonality can influence spatial epidemic spread and evolution. Hence, we consider the seasonal parameter, $\beta(t) = \beta_0(1 + \varepsilon \sin(2\pi t))$, where ε is the fluctuating amplitude of contact rate. Commonly, we describe the susceptibility, exposure, infection and recover process in terms of four nonlinear ODEs. We use S for susceptibles, E for the exposed, I for infectors, and R for the recovered. The dynamical equations for SEIR model are

$$\frac{dS}{dt} = \mu(1 - S) - \beta(t)IS, \quad (1a)$$

^{*}Electronic address: liuqx315@sina.com

[†]Electronic address: jinzhn@263.net

$$\frac{dE}{dt} = \beta(t)IS - (\mu + \delta)E, \quad (1b)$$

$$\frac{dI}{dt} = \delta E - (\gamma + \mu)I, \quad (1c)$$

$$\frac{dR}{dt} = \gamma I - \mu R. \quad (1d)$$

Here μ is the death rate per capacity, $1/\delta$ and $1/\gamma$ are the mean latent and infectious periods of the disease. $\beta(t)$ is the rate of disease transmission between individuals. The population can be normalized to $S + E + I + R = 1$, so all dependent variables represent fractions of the population. The original studies show that the system of (1) exist three phase transitions which are the stable behavior, the limit cycle and the chaotic behavior in the mean-field limit [18] with respect to the fluctuating amplitude, ε .

II. NEIGHBOURHOOD-DEPENDENT MODEL

Generally, studies on the spacial epidemic models show that there exists spatio-temporal travelling waves [20] (e.g. dengue haemorrhagic fever (DHF) [14, 21] and measles [13]). However, few systems are well enough documented to detect repeated waves and to explain their interaction with spatio-temporal variations in population structure and demography. The actual epidemic spread is spatio-temporal and local individual interact. Here we study the individual moving of the susceptible, exposed, infector and recover, and their diffusion from one lattice site to another. Then the equations (1) read

$$\frac{\partial S(\mathbf{r}, t)}{\partial t} = \mu - \beta(t)IS - \mu S + D_1 \nabla^2 S(\mathbf{r}, t), \quad (2a)$$

$$\frac{\partial E(\mathbf{r}, t)}{\partial t} = \beta(t)IS - (\mu + \delta)E + D_2 \nabla^2 E(\mathbf{r}, t), \quad (2b)$$

$$\frac{\partial I(\mathbf{r}, t)}{\partial t} = \delta E - (\gamma + \mu)I + D_3 \nabla^2 I(\mathbf{r}, t), \quad (2c)$$

$$\frac{\partial R(\mathbf{r}, t)}{\partial t} = \gamma I - \mu R + D_4 \nabla^2 R(\mathbf{r}, t). \quad (2d)$$

We study the system (2) using cellular automata method, which is suitable for modeling many reaction-diffusion systems in a quantitatively correct way based

on the Ref. [12], and demonstrate recurrent epidemic spiral waves or traveling waves in an exhaustive spatio-temporal through the numerical simulation. Simply, we use $\mathbf{c}(\mathbf{r}, t)$ to denote the vector of individual density in position \mathbf{r} and at time t , and $\mathbf{L}(\mathbf{c}(\mathbf{r}, t))$ to describe the local kinetics; \mathbf{D} is the diffusion coefficient matrix. Then the system (2) can be written as

$$\frac{\partial \mathbf{c}(\mathbf{r}, t)}{\partial t} = \mathbf{L}(\mathbf{c}(\mathbf{r}, t)) + \mathbf{D} \nabla^2 \mathbf{c}(\mathbf{r}, t). \quad (3)$$

In the following simulation, we may discard the equation (2d), since we concern the susceptible, exposed and infected.

We define this model as follows. Space is made up of a square lattice of $J \times J$. In each step the individuals randomly move in its neighborhood. The state of the cellular automata is given by a regular array of density vector \mathbf{c} residing on a two-dimensional lattice. We consider cellular automata with b_i states (denoted by the integers $0, 1, 2, 3, \dots, b_i$). Here species state 0 and b_i are zero population level and maximum population level respectively. The first step of each time iteration corresponds to local dynamics, and the state at each spatial lattice changes independently of the states at other vicinity lattices. The second part of each time step corresponds to unbiased spatial movement. The central operation of the cellular automaton consists of calculating the sum

$$\mathbf{c}_i(\mathbf{r}, t) = \sum_{\mathbf{r}' \in N_i} \mathbf{c}_i(\mathbf{r} + \mathbf{r}'). \quad (4)$$

Where the summation takes up all of the nearest neighbors of the cell \mathbf{r} . The neighborhoods can be different for each species i . We use the Moore neighborhood for all i in the two-dimensional space. i.e.

$$N_{square} = \{(0, 0), (1, 0), (0, 1), (-1, 0), (0, -1), (1, 1), (-1, 1), (1, -1), (-1, -1)\}. \quad (5)$$

We normalize values of $\mathbf{c}_i(\mathbf{r}, t)$, and the $\bar{\mathbf{c}}_i(\mathbf{r}, t) = \mathbf{c}_i(\mathbf{r}, t)/(b_i N_i)$ is local average density of the $\mathbf{c}_i(\mathbf{r}, t)$. The $\bar{\mathbf{c}}_i(\mathbf{r}, t)$ is always between zero and one.

From the Ref. [12], the two-dimensional discretization version of Eq. (3) takes the form

$$\mathbf{c}_i(\mathbf{r}, t + 1) = \mathbf{c}_i(\mathbf{r}, t) + \Delta t \mathbf{L}(\mathbf{c}_i(\mathbf{r}, t)) + D_i \nabla^2 \mathbf{c}_i(\mathbf{r}, t), \quad i = 1, 2, 3, 4. \quad (6)$$

Where the

$$D_i = D_{ii} \frac{\Delta t}{\Delta r^2}, \quad i = 1, 2, 3, 4. \quad (7)$$

and D_i defines the space scale.

Furthermore we have

$$\mathbf{c}_i(\mathbf{r}, t+1) = \mathbf{L}^*(\bar{\mathbf{c}}_i(\mathbf{r}, t)), \quad i = 1, 2, 3, 4. \quad (8)$$

Where $\mathbf{L}^*(\bar{\mathbf{c}}_i(\mathbf{r}, t)) = \bar{\mathbf{c}}_i(\mathbf{r}, t) + \Delta t \mathbf{L}(\bar{\mathbf{c}}_i(\mathbf{r}, t))$.

As $\mathbf{c}(\mathbf{r}, t)$ is the average output of the CA for the system (2), and therefore it is given by

$$c_j(\mathbf{r}, t+1) = \left\lfloor b_j L^* \left(\frac{c_i(\mathbf{r}, t)}{b_i N_i} \right) \right\rfloor + 1, \quad (9)$$

for species j . About $\mathbf{c}(\mathbf{r}, t)$ as output of the CA described in detail can be found in the paper [12].

III. NUMERICAL RESULTS

We have performed extensive numerical simulations of the described model, and the qualitative results are shown here. In cellular automata simulation, periodic boundary conditions are used and $\Delta t = 0.005$. The space scale $D_1 = 0.2$, $D_2 = 0.05$, $D_3 = 0.02$ and grid size used in the evolutionary simulations is 100×100 cells. Every species has 100 states in the system (2), and more states enable more accurately for discrete representation of the continuum models, while it is complex for analysis, and this is described in detail elsewhere [22]. We have tested that the larger grid size does not change qualitative result for the evolutionary dynamics. The contact rate fluctuates with the seasons can be approximated in several ways. Simply we choose sinusoidal force, $\beta(t) = \beta_0(1 + \varepsilon \sin(2\pi t))$, where $0 \leq \varepsilon < 1$, and another more realistic option is term-time force, which sets transmission rates high during school terms and low in other place [23]. The spatial patterns evolve from random initial conditions. The maximum density of susceptible levels, exposed levels and infected levels are set to 50, 5 and 1, respectively, in the two-dimensional space. Other initial conditions have been explored as well, and no change has been observed in the behavior. In Fig. 1 and Fig. 3 four different snapshots during the temporal evolution of the system are presented in two-dimensional space. These figures and the following figures are species density levels as a function of space and time on a gray scale, with white corresponding to the lowest-density state and black corresponding to the highest density state.

Fig. 1 and Fig. 3 have depicted spatial patterns in the two-dimensional space under different ε values (the fluctuating amplitude of contact rate) respectively. We have examined the temporal evolution by displaying successive time frame as a movie, but we are unable to represent this effectively on the printed page. From evolution snapshots (Fig. 1(a)-1(d)), one can see that there is no occurrence of spiral waves (fractal fronts) even if the system reaches a stable state when the ε is in certain interval. The certain interval is turned out to be $\varepsilon^* < \varepsilon < \varepsilon_c$ with the parameter value used in the figure and $\varepsilon^* \approx 0.048$ and $\varepsilon_c \approx 0.305$. Here the critical value $\varepsilon_c \approx 0.305$ in the spatial model (2), which is more than the value of the local

dynamic of the chaotic point of system (1) [18] (≈ 0.28). This result suggests another possible explanation, which is that populations embed and disperse more stably in space than they do in non-spatial counterparts [24, 25]. As the ε ($\varepsilon > \varepsilon_c$, in the domain of chaos) and time increase, the dynamical patterns with fractal fronts (spirals waves) of spatial structures occur, and become larger and more stable (see the Fig. 3). The CA models are generally based on qualitative rather than quantitative information about the system. It is hardly to detect the density calculated over the entire lattice when the system is enough larger. Hence, in order to investigate quantitatively the evolution of the system (2), we give the results by one-dimensional space. An explicit visualization of spatial organization within the lattice is provided by the space-time plot of Fig. 2 and Fig. 4.

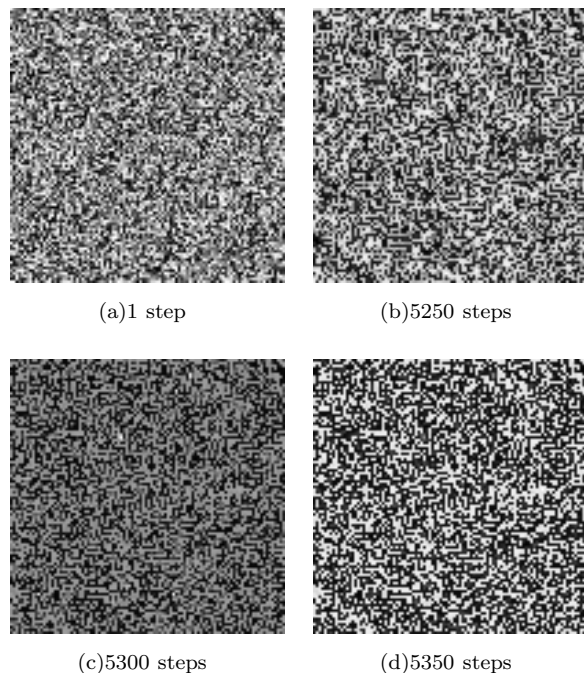


FIG. 1: A typical simulation shows four snapshots of the evolution in two-dimensional space with the parameters $\mu = 0.02$, $\delta = 35.84$, $\gamma = 100$, $\beta_0 = 1800$ and $\varepsilon = 0.23$. The figures plot susceptible density levels as a space on grey scale. The exposed and infected distribution has a qualitatively similar form.

In Fig. 2(a) the three time series displaying of the density of susceptible, exposed and infected for the first 10000 steps by CA are given. Self-sustained oscillations of the three time series develop (see the Fig. 2(a)). The amplitude of oscillations increase with the increase of fluctuating amplitude of the infection rate, ε (compared the Fig. 2(a) and 4(a)). In fact, large oscillations will lead to stochastic extinction of the species, when the value of fluctuating amplitude is more than ε_c in the domain of chaos. In Fig.2(b)-2(c), spatio-temporal pictures of the susceptible and exposed are plotted respectively, where

time increases from bottom to top and the horizontal axis represents the spatial location. From the Fig.2(b)-2(c), it is clearly seen that the whole system shows the spatial period-2 structure when the ε is between ε^* and ε_c (later we will give the case when ε is smaller than a critical value ε^*).

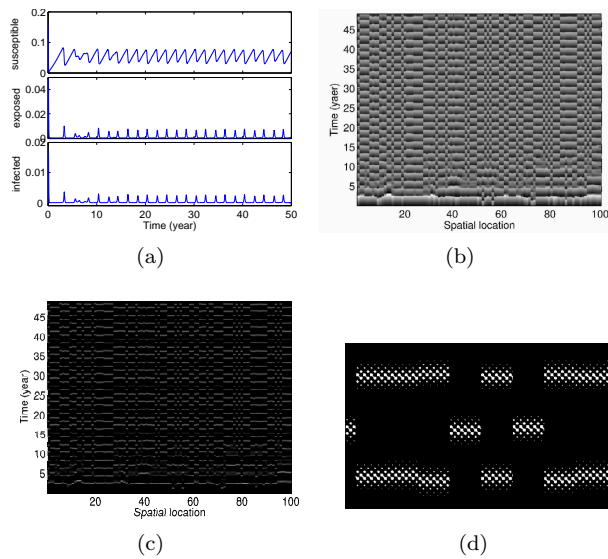


FIG. 2: The spatial period-2 structure results for the system (2) in one-dimensional space in cellular automaton models and the parameters are the same as those in Fig. 1. We use a spatial domain of 100 lattices; 10000 successive time iterations are plotted. In (a) we show the species density as a function of time. The figure (b) and (c) show the susceptible and exposed density levels as a function of space and time on a grey scale respectively. The behavior of the infected is qualitatively similar. At this scale the spatial discretization is not really visible, and therefore we have enlarged one region of the plane in figure (c) as figure (d), in order to illustrate this discretization.

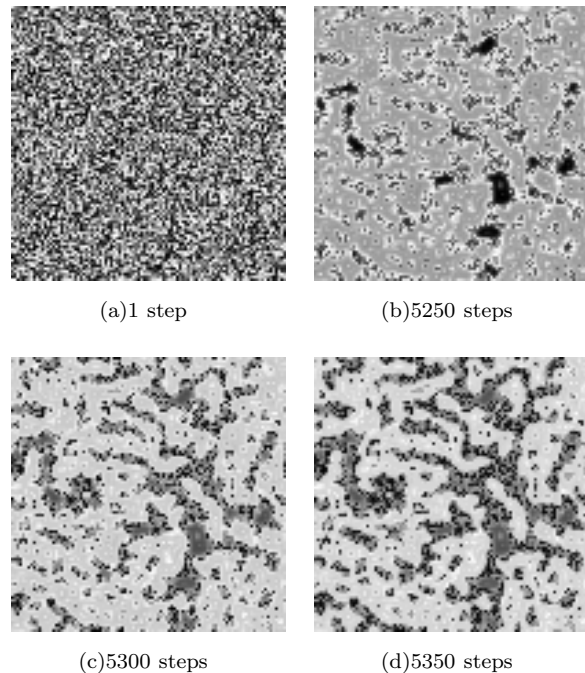


FIG. 3: A typical simulation shows four snapshots of the evolution in two-dimensional space. The parameters are the same as in Fig. 1, $\mu = 0.02$, $\delta = 35.84$, $\gamma = 100$, $\beta_0 = 1800$ and $\varepsilon = 0.38$. The figures plot susceptible density levels as a space on grey scale. The exposed and infected distribution has a qualitatively similar form.

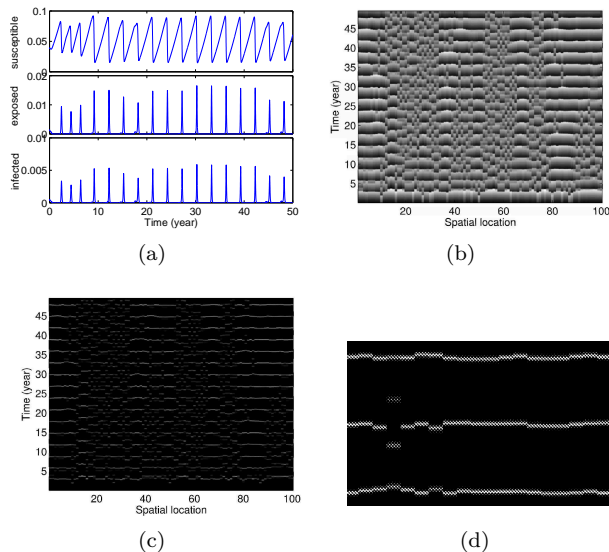


FIG. 4: The spatial period-2 structure results for the system (2) in one-dimensional cellular automata models and the parameters are the same as those in Fig. 3. We use a spatial domain of 100 lattices; 10000 successive time iterations are plotted. In (a) we show the species density as a function of time. The figure (b) and (c) show the susceptible and exposed density levels as a function of space and time on a grey scale respectively. The behavior of the infected is qualitatively similar. At this scale the spatial discretization is not really visible, and therefore we have enlarged one region of the plane in figure (c) as figure (d), in order to illustrate this discretization.

To furtherly investigate the impact of the fluctuating amplitude on the dynamical patterns with fractal fronts (or spiral waves) in two-dimensional and the spatial period-2 structure in one-dimensional space respectively, we study the case when the SEIR model is deeply in the domain of chaos and out of the domain of chaos. The evolution of system (2) is shown with $\varepsilon = 0.38$ in Fig. 3 and Fig. 4. In Fig. 3(b)-3(d) three snapshots are taken at 5250, 5300 and 5350 steps respectively. In Fig. 3(b) the rotating spirals are not recognizable due to the irregular interfaces. However, the spiral formation becomes visible when the interfacial roughness grows by the infected invasion as demonstrated in Fig. 3(d). In Fig. 3(d) one can easily identify the vortices and antivortices rotating clockwise and counterclockwise, respectively. We have to emphasize that this pattern cannot be characterized by a single length unit (e.g., correlation length) because the main features of spirals (armlength, average curvature, average distance, etc.) depend on the model parameters. But it may be analysed by using some geometrical features method [26]. The armlength of these spiral waves are broad and do not easily break, resulting in periodical recurrence of epidemic waves. The spontaneous formation of spiral waves means the regularly recurrent infection waves (Fig. 3(a)-3(d)). Similarly the

irregular spiral waves can also be observed even when the fluctuating amplitude is much more than the critical value ε_c . These results are not shown in this paper.

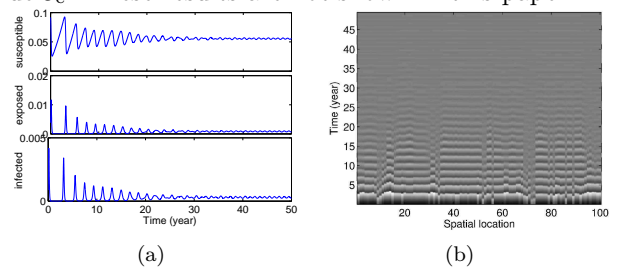


FIG. 5: The spatio-temporal evolution of the system (2) in one-dimensional cellular automata models for the $\varepsilon < \varepsilon^*$ case, $\varepsilon = 0.035$. In (a) we show the species density as a function of time. The figure (b) is plot susceptible density as a function of space and time on a grey scale. The behavior of the exposed and infected is qualitatively similar.

Figure 5 shows the time evolution of the density of the species and the spatio-temporal configurations of the system (2) at $\varepsilon = 0.035$. The spatio-temporal evolution of the expose and infected are similar with the susceptible's (Figure 5(b)). It can be clearly noticed that spatial period-2 structure disappear and the stationary state is a fixed point with the decreasing of ε . The situation corresponds to a low and persistent endemic infection in Fig. 5(a). The oscillations decay to the fixed point when the ε is smaller than the critical value ε^* case. The oscillations decay because these infection clusters grow, the availability of infected hosts per susceptible host is reduced, decreasing the number of new infectors. In this case, the spontaneous formation of dynamical patterns is qualitatively similar in Fig. 3 in two-dimensional.

IV. CONCLUSIONS

A realistic spatial epidemic with the individuals randomly moving in its neighborhood has been modeled using cellular automata. Our simulations demonstrate that the recurrent infectious waves exist and persist in an exhaustive spatio-temporal. We have investigated the dynamical patterns of system (2) in one and two dimensions respectively. We show that the spiral waves recur periodically and the recurrence is insensitive to the change of the fluctuating amplitude ε within the domain of chaos (the fluctuation amplitude $\varepsilon > \varepsilon_c$). Moreover the dynamical patterns with fractal fronts grow stably. The system also shows spatial period-2 structure in one dimension when ε is between ε^* and ε_c outside the domain of chaos. It is interesting that the spatial period-2 structure will break and transform to spatial synchronous configuration in the domain of chaos. Our results confirm that populations embed and disperse more stably in space than they do in non-spatial counterparts.

Acknowledgments

This work was supported by the National Natural Science Foundation of China under Grant No 10471040

and the Science Foundation of Shan'xi Province No 2006011009.

-
- [1] P. Rohani and O. Miramontes, Proc. Roy. Soc. Lond B **260**, 335 (1995).
- [2] A. Provata and G. A. Tsekouras, Phys. Rev. E **67**, 056602 (2003).
- [3] G. A. Tsekouras and A. Provata, Phys. Rev. E **65**, 016204 (2001).
- [4] A. Provata, G. Nicolis, and F. Baras, J. Chem. Phys. **110**, 8361 (1999).
- [5] J. S. Nicholas and P. Hogeweg, Proc Roy. Soc. Lond. B **265**, 25 (1998).
- [6] W. S. C. Gurney, A. R. Veitch, I. Cruichshank, and G. Mcgeachin, Ecology **79**, 2516 (1998).
- [7] J. D. Murray, *Mathematical Biology* (Springer-Verlag Berlin Heidelberg, 1993).
- [8] R. M. Anderson and R. M. May, Nature **318**, 323 (1985).
- [9] R. M. Anderson and R. M. May, Science **215**, 1053 (1982).
- [10] U. Dieckmann, R. Law, and J. A. J. Metz, *The Geometry of Ecological Interactions: Simplifying Spatial Complexity* (Cambridge University Press, United Kingdom, 2000).
- [11] J. A. Sherratt, B. T. Eagan, and M. A. Lewis, Phil. Trans. Roy. Soc. Lond. B **352**, 21 (1997).
- [12] R. J. Weimar and B. Jean-Pierre, Phys. Rev. E **49**, 1749 (1994).
- [13] B. T. Grenfell, O. N. Bjørnstad, and J. Kappey, Nature **414**, 716 (2001).
- [14] D. A. T. Cummings, N. E. Huang, T. P. Endy, A. Nisalak, and B. D. S. K. Ungchusak, Nature **427**, 344 (2004).
- [15] T. Antal, M. Droz, A. Lipowski, and G. Ódor, Phys. Rev. E **64**, 036118 (2001).
- [16] M. Droz and A. Pekalski, Physica A **298**, 545 (2001).
- [17] W. M. van Ballegooijen and M. C. Boerlijst, Proc. Nati. Acad. Sci. **101**, 18246 (2004).
- [18] L. F. Olsen and W. M. Schaffer, Science **249**, 499 (1990).
- [19] B. T. Grenfell, A. Kleczkowski, S. P. Ellner, and B. M. Bolker, Phil. Trans. Roy. Soc. Lond. A **348**, 515 (1994).
- [20] S. Djebali, Nonl. Anal.: Real World Applications **2**, 417 (2001).
- [21] A. Vecchio, L. Primavera, and V. Carbone, Phys. Rev. E **73**, 1913 (2006).
- [22] J. A. Sherratt, Physica D **95**, 319 (1996).
- [23] J. D. E. David, P. Rohani, M. B. Benjamin, and B. T. Grenfell, Science **287**, 667 (2000).
- [24] M. P. Hassell, H. N. Comins, and R. M. May, Nature **353**, 255 (1991).
- [25] P. Rohani and O. Miramontes, Proc. Roy. Soc. Lond. B **260**, 335 (1995).
- [26] G. Szabó and A. Szolnoki, Phys. Rev. E **65**, 036115 (2002).